ULTRAMINIATURIZED MILLIWATT-SCALE PERMANENT MAGNET GENERATORS

F. Herrault[1,2], C.-H. Ji[1], R.H. Shafer[1], S.-H. Kim[1], and M.G. Allen[1]
[1] Georgia Institute of Technology, Atlanta, Georgia, USA
(Tel: +1-404-894-9909, Email: fh59@mail.gatech.edu)
[2] Institut National des Sciences Appliquées de Toulouse, Toulouse, FRANCE

Abstract: This paper reports the design, fabrication and experimental characterization of ultraminiaturized, axial-flux, permanent-magnet (PM) generators intended for milliwatt range systems. The miniaturization of PM machines is attractive because scaling laws are favorable, but integration of ultra-small permanent magnets is challenging. The generators are 2-pole, multi-turn, 2-mm diameter machines. A single-phase, open-circuit voltage of $51mV_{rms}$ has been measured at 392krpm, which approximately corresponds to 3.6mW of DC power to a load resistance at the point of maximum power transfer, indicating that this approach shows great promises for milliwatt-scale power devices.

Keywords: Microscale generator, power MEMS, permanent-magnet machine, corrosion effects.

1. INTRODUCTION

MEMS-based magnetic generators/motors are very attractive as the mechanical-to-electrical transducer of compact, self-contained power generation systems. Appropriate mechanical input can be provided by micro-gas-engines [1], high-pressure gas sources, distributed fluidics (e.g., pipeline monitoring), or energy scavenging. We previously reported a 10-mm-scale, micromachined permanent-magnet (PM) generator that delivers 8W of DC power to a resistive load at a rotor speed of 305krpm [2]. In this paper, we investigate mW-scale, ultraminiaturized PM generators. Such machines can be applied to backup battery chargers, ubiquitous sensor networks, and RF MEMS. 2-mm, 2-pole, multi-turn, 3-phase machines have been fabricated, and electrically characterized.

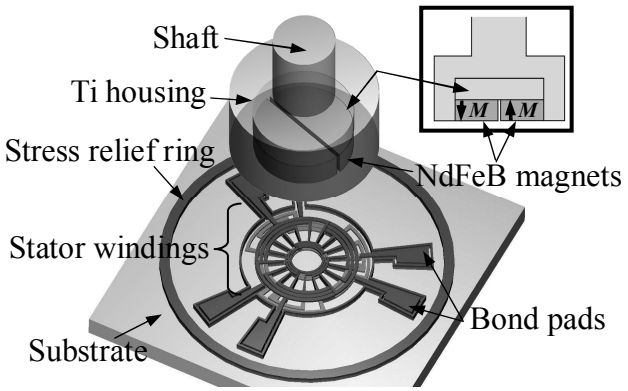

Fig. 1 Renderings of a 2-pole, 3-turn, 2-mm stator, and 2-pole, NdFeB rotor.

2. MINIATURIZATION CONSTRAINTS

Scaling analysis based on the previously reported 10 mm scale machine shows that 2-mm-scale machines (Fig. 1) can provide appreciable mW-scale electrical power. However, microfabrication of the device, and associated magnetics becomes more challenging, and this can be a key design driver leading to unconventional design choices for optimal performance. For example, consider the design choice of number of poles in the magnetic machine. In a multi-pole magnetic rotor, the per-pole extent of oxidized zones or N-S pole transition regions (which do not contribute to power generation) can be tens to hundreds of microns per pole. The total lateral extent of these unproductive regions is small compared to the perimeter of a cm-scale or larger rotor, but a significant fraction of the perimeter of a mm-scale rotor.

Although microfabricated permanent magnets show great promise for ultrasmall devices [3,4], relatively low achievable thicknesses limit their use in mW-scale power generation. Hence, 0.5-mm thick, commercially available sheets of NdFeB are used. Two halves of 2-mm diameter demagnetized discs are machined by IR laser under a nitrogen blanket to minimize corrosion. A 10-μm thick nickel coating layer is then deposited by electroless plating to act as an oxidation barrier. The corrosion resistance efficacy of this layer is tested by immersing the magnet in an HCl bath to accelerate the potential damage, and by

tracking the weight loss of the PM pieces as a function of time [5]. Results in Fig. 2 confirm that the corrosion resistance of the coated magnets is much higher than that of uncoated magnets. Finally, the pieces are fully magnetized using a conventional discharge-capacitance magnetizer and assembled together with a 0.5-mm thick, 2-mm diameter FeCoV back iron disc into a titanium rotor housing.

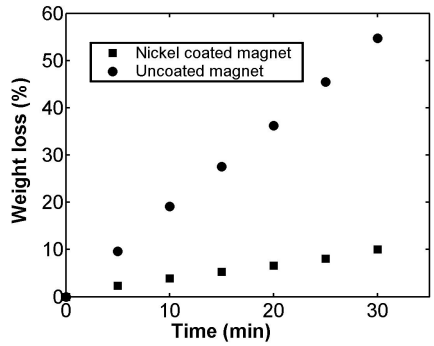

Fig. 2 Accelerated corrosion test result of uncoated and coated NdFeB permanent magnets.

The designed machines are two-pole, which minimize the number of magnetic transition regions, 3-phase, axial-flux, synchronous devices. Four different stator designs have been tested, as presented in Fig. 3.

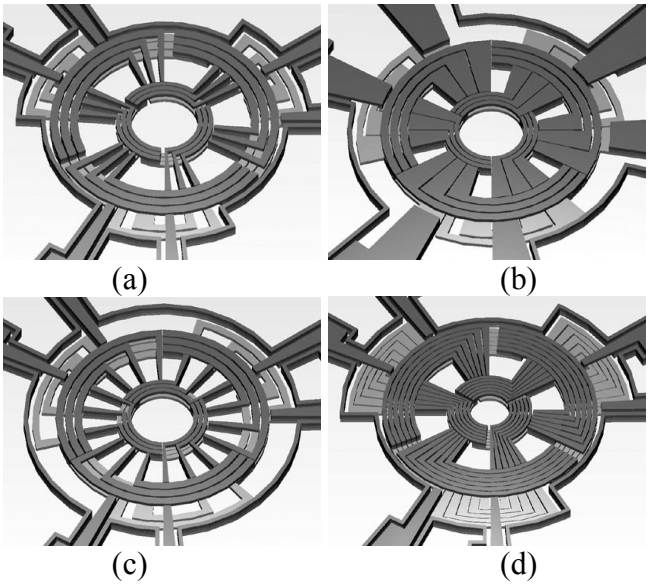

Fig 3 Stator designs: (a~c) 23(A~C), and (d) 26.

The denominations of the stators correspond to the number of poles, and the number of turns of each stator design. Thus, the designs 23(A~C), and 26 are 2-pole, 3-turn, and 2,-pole, 6-turn stators, respectively. 23B design has wider radial conductors than 23A, and 23C, which decreases the conduction losses. The radial conductors of 23A are packed per phase, while the ones of 23C are evenly distributed.

3. FABRICATION

The microfabricated surface-wound windings have two electrodeposited copper layers of 10-15μm thickness, embedded in an SU-8 epoxy mold. Fig.3 shows Scanning Electron Microscopy (SEM) images of the design 23C. The SU-8 mold has been etched away for imaging purposes.

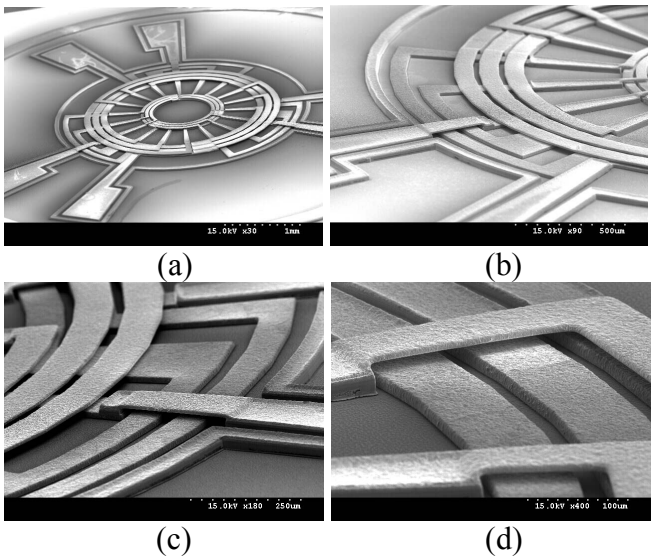

Fig. 4 SEM images of a 23C stator. (a) Full view, (b~d) Close-ups on the layers winding.

The copper windings are then released from the silicon substrate by underetching the silicon dioxide, and glued with a thin insulating layer of SU-8 onto a high permeability NiFeMo substrate. This magnetic substrate acts as a stator back iron, and will maximize the open-circuit voltage. Even though the output voltage delivered by the stators fabricated onto a silicon substrate is expected to be lower than that of the stators transferred onto the magnetic substrate, measurements have been performed using both types of machines. The fabricated stator die is glued onto a ceramic package, and wire-bonded for testing, as shown in Fig. 5.

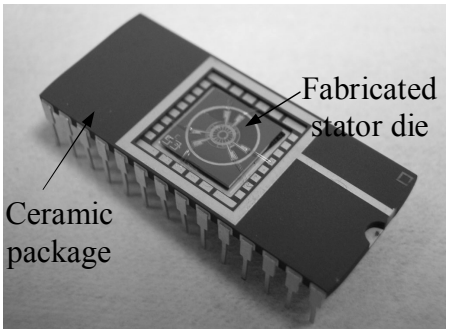

Fig.5 Fabricated stator windings mounted and wire-bonded in ceramic package.

4. ELECTRICAL CHARACTERIZATION

The rotor is spun above the microfabricated copper windings (Fig. 6) using an off-the-shelf air-driven turbine. The air gap, and the relative position of the stator to the rotor are set using xyz micropositioners. Maximum speed is limited by the turbine performance and not by the failure of the magnets as in large scale machines [1].

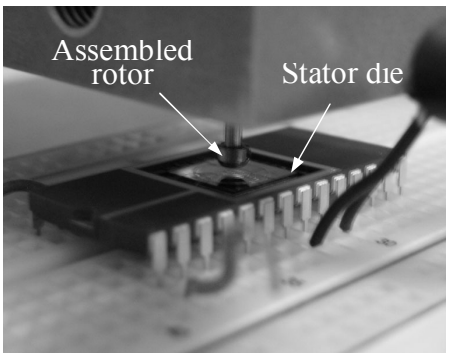

Fig. 6 Close-up of the microgenerator in operation. The stator package is mounted on an xyz-stage.

By analyzing the open-circuit voltage of the machines, one can extract the rotational speed of the rotor and the estimated DC output power. If any losses in the power electronics are neglected, the DC output power delivered at the point of maximum transfer can be calculated using Eq. (1).

$$P_e = \frac{3}{4} \times \frac{V_{oc}^{\ 2}}{(R_w + 2 \times R_{pin} + 2 \times R_c)}. \qquad (1)$$

where P_e is the DC output electrical power, V_{oc} is the open-circuit voltage, R_w is the winding resistance, R_{pin} is the package pin resistance, and R_c is the resistance of the Al wire connections. The factor 3 comes from the 3 phases, and the coefficient 1/4 assumes matched load conditions (Thevenin theorem). The rotor speed is measured using the electrical frequency of the open-circuit voltage waveforms. For 2-pole PM machines, an operating electrical frequency of 1.67kHz corresponds to a rotational speed of 100,000rpm and a velocity of 60m/s. The same rotor has been used throughout the testing of different devices. The minimum operating air gap is set by bringing the stator right before it blocks the spinning rotor.

5. DISCUSSION

The air gap is estimated at approximately 50μm. Table 1 summarizes the results for the different machines that have been tested. The copper packing density is defined as the area occupied by the radial copper conductors over the total area (outer and inner diameters of the radial conductors).The single phase winding inductance and resistance are measured in the 1kHz-100kHz frequency range using an impedance analyzer. The values compare favorably to simulated values with the respective thicknesses of the two copper layers. The discrepancy can be attributed to local shape and material property differences of the fabricated device and the model. The 23(A~C) devices exhibit approximately the same open-circuit voltage. Even though the open-circuit voltage of the 6-turn device is much higher, its large resistance drastically decreases the mechanical-to-electrical power. One of the 23B devices, "23B_C11", was transferred onto a NiFeMo substrate. A 4x improvement of the mechanical-to electrical power conversion has been measured between 23B_A11 and 23B_C11.

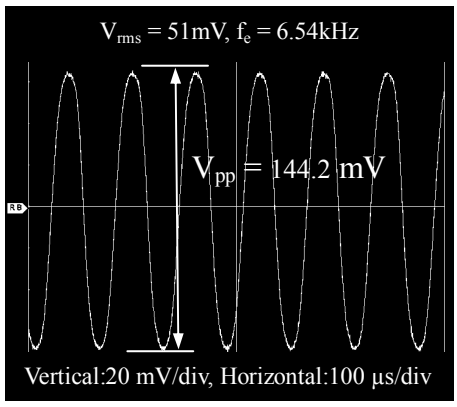

Fig. 7 Single phase open-circuit voltage waveform from 23B_C11 at 392 krpm.

Table 1 Comparison of several 2-pole microgenerators

Machine Type_#	Copper Packing Density	Measured Resistance (Simulation) (mΩ)	Measured Inductance (nH)	Open-circuit Voltage (mVrms)	Mechanical-to-electrical Power Conversion (mWatts)	Calculated Output Power (mWatts)
23A_D10	21%	416 +/-2 (428)	17 +/-3	27.7	2.76	0.95
23B_A11	71%	342 +/-3 (349)	18 +/-3	25.4	2.83	0.9
23C_A4	21%	467 +/-5 (443)	16 +/-3	25.5	2.09	0.75
26_C8	42%	1328 +/-95 (1192)	61 +/-5	49.9	2.81	1.25
23B_C11	71%	343 +/-7 (349)	18 +/-3	51	11.4	3.6

The 23B_C11 machine delivers 51mVrms (Fig. 7) at a rotational speed of 392krpm from a single phase, which corresponds to 11.4mW of mechanical-to-electrical power conversion. The open-circuit voltage is linear as a function of the rotor speed, and decreases as the gap increases, as depicted in Fig. 8.

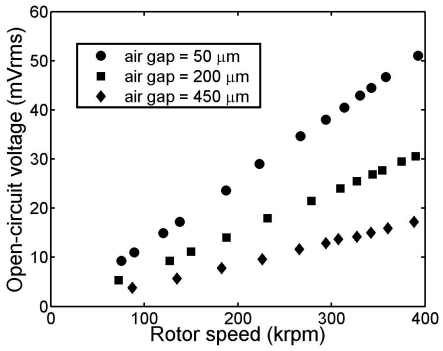

Fig. 8 Single phase, open-circuit voltage of 23B_C11 as a function of the rotor speed for several air gaps.

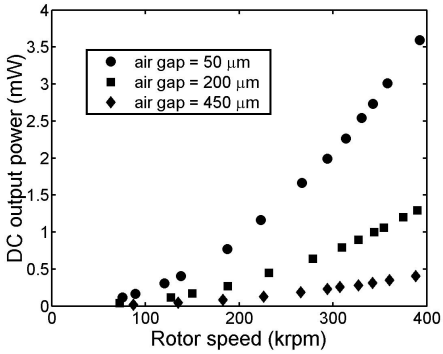

Fig. 9 Calculated DC output power across a resistive load.

An additional resistance of approximately 200mΩ per phase comes from the packaging (~40-50mΩ from each package pin, and 50mΩ from each connection). By taking it into account, there is approximately 3.6mW of DC power capability across a load resistance at the point of maximum power transfer (Fig. 9).

CONCLUSIONS

Ultraminiaturized PM generators have demonstrated a maximum open-circuit voltage of $51mV_{rms}$ at 392 krpm, corresponding to an estimated DC output power of 3.6mW. These promising results indicate that ultrasmall magnetic generators are a feasible approach to the generation of mW-scale power. The packaging however, must be improved to decrease the electrical losses, and maximize the efficiency of the whole machine. Next steps will include the development of an AC/DC converter.

REFERENCES

[1] S. A. Jacobson and A. H. Epstein, "An informal survey of power MEMS," *Proc. Int. Symp. Micro-Mechanical Eng. 200*3, pp. 513-520.

[2] D. P. Arnold, F. Herrault, I. Zana, P. Galle, J.-W. Park, S. Das, J. H. Lang, and M. G. Allen, "Design optimization of an 8 W, microscale, axial-flux, permanent-magnet generator," *J. Micromech. and Microeng*, v 16, n 9, Sept. 2006, p S290-6.

[3] T. Budde, H. H.Gatzen, "Magnetic properties of an SmCo/NiFe system for magnetic microactuators," *J. Magnetism and Magnetic Materials,* v. 272-276 May 2004, p.2027-8

[4] A. Walther, K. Khlopkov, F. May, N. Dempsey, and O. Gutfleusch, "Magnetic and microstructural properties of thick sputtered NdFeB films," *Intermag 2006,* pp. 223.

[5] Z. Chen, A. Ng, J. Yi, and X. Chen, "Multi-layered Electroless Ni-P coatings on powder-sintered Nd-Fe-B permanent magnet," *J. Magnetism and Magnetic Materials,* v 302, n 1, July 2006, p 216-22